Tracking of Cell Nuclei for Assessment of In Vitro Uptake Kinetics in Ultrasound-Mediated Drug Delivery using Fibered Confocal Fluorescence Microscopy

Marc Derieppe, Baudouin Denis de Senneville, Hugo Kuijf, Chrit Moonen, Clemens Bos

Title

Tracking of Cell Nuclei for Assessment of *In Vitro* Uptake Kinetics in Ultrasound-Mediated Drug Delivery using Fibered Confocal Fluorescence Microscopy

Authors

Marc Derieppe[1], Baudouin Denis de Senneville[1,2], Hugo Kuijf[1], Chrit Moonen[1], Clemens Bos[1]

Affiliations

[1]Imaging Division

University Medical Center Utrecht

Heidelberglaan 100, P.O.

Box 85500, 3508 GA Utrecht, Netherlands

[2]Institut de Mathématiques de Bordeaux

UMR 5251 CNRS - Université Bordeaux 1 - INRIA

Bordeaux, France

Correspondence: c.moonen@umcutrecht.nl - Tel: +31 887 550 274

Abstract

Purpose. Previously, we demonstrated the feasibility to monitor in real-time the ultrasound-mediated uptake of a cell-impermeable model drug with fibered confocal fluorescence microscopy. Here we present a complete post-processing methodology in order to improve the accuracy of the measured pharmacokinetic parameters.

Procedures. After the detection of the nuclei based on a radial symmetry transform algorithm, a frame-by-frame tracking allowed for the monitoring of each individual uptake. The resulting pharmacokinetic parameters were derived from a two-compartment model.

Results. With the tracking, 93% of the 370 nuclei showed a fluorescence signal variation that was well described by a two-compartment model. For each kinetic parameter, the tracking allowed for more homogeneous distributions.

Conclusions. This post-processing methodology improved the accuracy of the uptake pharmacokinetic parameters assessed in a cell population. This study extends the proof of concept of designing an *in vitro* setup for the real-time monitoring of an US-mediated model drug uptake.

Key Words: drug delivery, pharmacokinetic parameters, biological barrier, plasma membrane permeabilization, ultrasound bioeffects, fibered confocal fluorescence microscopy, single-nucleus tracking.

Introduction

Local drug delivery for the treatment of solid tumors [1] aims at depositing a high dose of anticancer agent in the tumor tissue while limiting toxic side effects, e.g. cardiotoxicity [2]. A key step is the crossing of biological barriers, such as the endothelial barrier [3][4] and the plasma membrane for drugs that need to bind DNA. This prerequisite is only partly fulfilled for hydrophilic anticancer agents, e.g. cisplatin and bleomycin, and it has been proposed to use plasma membrane permeabilization techniques, especially electroporation [5][6] or sonoporation using ultrasound (US) waves [7][8][9], to increase the proportion of drug binding to DNA, thus becoming effective.

Fluorescence microscopy is a good candidate to investigate the kinetics of US-enhanced uptake as it allows studying biological processes at the cellular and molecular scale. Modern fluorescence microscopy systems are capable of imaging with high spatial resolution and temporal resolution, which specifically enables resolving the dynamics and kinetics of these processes [10]. Dynamic microscopy has for example been used to monitor molecular motors involved in intracellular dynamics [11][12][13], plasma membrane dynamics [14], and nuclear mechanisms [15][16]. Analysis of these time series requires application-specific image post-processing. To study uptake kinetics, we recently demonstrated [17] the potential of a setup consisting of a Fibered Confocal Fluorescence Microscopy (FCFM) system, offering minor geometrical constraints, an ultrasound- and optical- compatible cell culture chamber, and an unfocused ultrasound transducer. This setup allowed assessing the uptake of a model drug, i.e. SYTOX Green intercalating fluorescent dye after sonoporation. In this preliminary study, we monitored the fluorescence signal enhancement of individual nuclei, but we did not take nucleus motion into account. For that reason, we monitored the signal attributed to a nucleus based on the single pixel that had the highest intensity in order to

monitor the same maximum in the region of interest (ROI), thus limiting the impact of potential nucleus displacement.

Here we present a post-processing methodology that addresses these limitations, including tracking of nuclei from frame to frame in order to improve the accuracy of the measured kinetic parameters. Specifically, the proposed method consists of 1) pre-processing designed to improve the precision and the accuracy of the acquired data, 2) detection of the nuclei based on a radial symmetry transform algorithm, 3) frame-by-frame tracking of detected nuclei, which allowed for the monitoring of each individual uptake, 4) fitting of a two-compartment model to the intensity data to assess the kinetic parameters, 5) statistical analysis of the resulting population kinetic data. We then demonstrate that this methodology allows for the study of kinetic parameters in a cell population of more than hundred cells per experiment.

Materials and Methods

Setup and experimental protocol

In this study, the data were collected using the protocol proposed in Derieppe *et al.* [17]. Briefly, the *in vitro* setup consisted of a 37°C waterbath containing a 1.5 MHz unfocused monoelement transducer (0.88 MPa peak-to-peak pressure, 20% duty cycle, 1 kHz pulse repetition frequency, 1W electrical effective power, 30 second exposure time). C6 rat glioma cells were seeded in an ultrasound compatible cell culture chamber (OptiCell™, Thermo Fischer Scientific, Rochester, NY, USA). Cells were then exposed to US waves in the presence of a commercially available ultrasound contrast agent (Sonovue, Bracco, Milan, Italy) at an average concentration of 10 microbubbles per cell. The tip of the FCFM microprobe was in contact with the upper wall of the culture chamber, and allowed monitoring the uptake of SYTOX Green fluorescent dye (excitation/emission = 504/523 nm, Molecular weight = 600 Da), by means of the fluorescence signal intensity.

Signal collection

On the single channel FCFM images, cell nuclei present as high intensity spots with a circular shape whose radius typically ranges from 4 to 10 µm (cf. supplementary data, video 1, video 2, and video 3). Therefore, the spatial mean signal for each nucleus was calculated from a 4-pixel-radius (4.8 µm) circular ROI, centered on the intensity-weighted center of mass of the nucleus.

Evaluation of the impact of nucleus displacement on the measured signal

Numerical simulations (MATLAB® 2010 - MathWorks, USA) were conducted to estimate the impact of nucleus displacement on the measured signal. As was observed experimentally, the cell nucleus was modeled to have a Gaussian fluorescence signal profile with a full width at

half maximum ranging from 4 µm to 10 µm. The signal loss ratio was calculated from the 2-dimensional convolution of the nucleus signal with a stationary 2-dimensional circular window function representing the stationary ROI (Fig. 1a), as a function of nucleus displacement.

Single-nucleus tracking

Automated single-nucleus tracking (SNT) was implemented to take into account cell motion and improve the accuracy of signal intensity monitoring. In accordance with the general framework described by Meijering et al. [18], the SNT methodology included preprocessing of image data, detection of individual nuclei, definition of frame-to-frame correspondence of nuclei, and analysis of the results.

SNT – Image data preprocessing

Data post-processing was conducted with custom scripts and standard routines written in IDL 8.0 (Exelis Visual Information Solutions). TIFF-format images were extracted from proprietary .mkt images (Mauna Kea Technologies, Paris, France). First, frames were resampled to 1-second temporal resolution from the acquisition frame rate (i.e. 8.5 frames/s) set by default by the acquisition hardware, by averaging the frames acquired within 1 second; This improved the Signal-to-Noise Ratio (SNR) of the data while decreasing the calculation time and the memory usage required by the SNT. Second, the first frame acquired before the US exposure was subtracted on a voxel-by-voxel basis from the rest of the frames to compensate for the systematic bias caused by fiber-bundle auto-fluorescence. Then, the SNR was further improved by means of anisotropic filtering using the Smallest Univalue Segment Assimilating Nucleus (SUSAN) filter [19], in order to detect nuclei at an early stage of signal enhancement. The SUSAN filter only was applied on the image background. A 20-pixel

square Gaussian kernel with a 2.5-pixel standard deviation was applied, which is substantially less than the apparent size of the cell nuclei on FCFM.

Single nucleus tracking – individual nucleus detection

The cell nuclei were detected using the radial symmetry transform (RST) algorithm from Loy et al. 2003 [20][21]. First, the normalized gradient image was computed by convolution with the Sobel kernel. The RST then counts the number of gradient vectors pointing at the pixel of interest by evaluating its neighbors one-by-one; this counting was restricted to a radius range set from 3 to 8 pixels, i.e. from 4 to 10 µm, and weighted by the gradient image magnitude. The normalization parameter (Kappa) was set at 9.9, in accordance with Loy et al. [20], to compensate for the higher probability for large cell nuclei to have a greater number of gradient vectors pointing at it, based on size only. The radial strictness parameter (Alpha) was set at 1 to allow imperfect circular shapes of the nuclei. A radial symmetry matrix was then computed for each nucleus radius within the range set. Each symmetry matrix was convolved by a 2-dimensional Gaussian kernel in order to leave a single center of mass for each nucleus. The full width at half maximum of the Gaussian kernel was set to a quarter of the radius of the nucleus. Finally, the resulting radial symmetry matrices were combined in a single 2-D symmetry matrix integrating the information from all scales [20].

A thresholding allowed creating a binary mask for each frame in order to locate the cell nuclei. A 100-unit threshold was found to give a balance between detecting nuclei at an early stage, and minimizing the number of merged nuclei for all datasets. Note that the nuclei were not tracked until the corresponding 2-D symmetry matrix reached the threshold detection limit. For each frame, each detected region could then be labeled. The corresponding coordinates of each intensity-weighted center of mass were calculated, and used as the input for the SNT algorithm.

SNT – Frame-by-frame nucleus correspondence

Since the acquisition frame rate was high compared to the cell motion, the iterative closest point method (ICP) [22] was employed to determine the frame-by-frame nucleus correspondence. We will use an analogy with the family tree to describe the link between a nucleus in one frame, referred to as "the parent", and the corresponding nucleus in the next frame, "the child". This correspondence was determined in time-reversed order to ensure the presence of all nuclei in the starting frame of the SNT, i.e. the last frame of the sequence.

Two scenarios were then addressed that introduce ambiguity, namely "merging" and "splitting".

"Merging": nuclei in close proximity of each other that are not resolvable any longer are detected as a single spot; This hampers unraveling the frame-by-frame correspondence. In this scenario (Fig. 2a), the nuclei detected in frame t-1 are detected as a single region in frame t. Nuclei involved in merging were detected by first listing nuclei without child (step 1). Merging partners were then defined using a forward ICP (step 2). Each lineage was finally discarded, since the measured signal evolution for these nuclei was potentially inaccurate, and might bias the estimation of the population kinetic parameters (step 3).

"Splitting": This scenario (Fig. 2b), arises from the fact that two children (reported in frame t-1) can possibly be linked to an identical parent in frame t-2 (step 1). This will be an extremely rare event, since a nucleus is unlikely to divide during the acquisition. An ICP allowed determining the real child (step 2) and the link between the parent and his other child was discarded (step 3).

Verification step by the operator

In line with Meijering et al. [18] an operator verification step was implemented. Pathological cases can be linked to some typical scenarios, which are listed below, with the consequence for the signal behavior in parentheses: nuclei entering the field of view during the acquisition and merged nuclei that split during the acquisition (fluorescence signal enhancement occuring late in the signal profile), multiple clustered nuclei that are detected as a single nucleus from the beginning to the end of the acquisition (oscillating fluorescence signal profile due to the position fluctuations of the intensity-weighted center of mass). Pathological cases were identified by reviewing the video provided for each dataset (cf. supplementary data, video 1, video 2 and video 3) as well as the signal profile over time of the individual nuclei.

The remaining nucleus subpopulation served as the basis for the statistical analysis.

Single nucleus tracking – Results analysis

After nucleus tracking, analysis of the fluorescence signal intensity over time was performed to extract parameters describing the uptake kinetics. A two-compartment model, with an extracellular and an intracellular compartment separated by a plasma membrane, was proposed to analyze the fluorescence signal enhancement of the individual cells. For this system, the time-dependence of the mean intensity is given by:

$$I(t) = A[1 - e^{-k(t-T)}] \text{ (1)},$$

where A is the asymptotic signal enhancement, T the time of fluorescence signal onset, and k the transfer rate constant. These kinetic parameters were obtained from a Levenberg-Marquardt least-square fit applied to the fluorescence intensity of individual nuclei over the 9-minute sequence. The goodness of the fit was evaluated by means of Pearson's correlation coefficient (r^2). The model was considered accurate when r^2 was greater than 0.95. The signal enhancement and uptake rate constants were derived from this fit. For the saturation signal,

values were normalized to the mean saturation signal with tracking, in order to evaluate biases and heterogeneity. Fluorescence signal onset, however, was defined as the time when the nucleus signal exceeded the noise level by five standard deviations. The standard deviation was determined from a 5-second baseline acquired before the onset of the US exposure. In order to circumvent the detection limit, which made it impossible to assess the signal level at the very early stage of the signal enhancement, the ROIs computed for the newly detected nuclei were propagated at the same location to the previous frames, for a more accurate signal monitoring (Fig. 4, blue profile). The propagation of these ROIs only served for the assessment of the signal onset.

Data are presented as median (interquartile range – number of samples). For each pharmacokinetic parameter, the distributions with and without tracking have been compared using the Wilcoxon matched-pairs signed rank test. The impact of the verification by the operator has been evaluated using the unpaired nonparametric Mann-Whitney test and was considered significant when $p < 0.05$.

Results

Impact of cell nucleus displacement on the measured signal

The proposed numerical simulation showed that nucleus displacement significantly influences measured fluorescence intensity, due to poor overlap of the region of interest (ROI) used for signal summation and the actual location of the cell (Fig 1a). A 20% signal loss for a 4 µm FWHM nucleus and 25% signal loss for a 10 µm FWHM nucleus are seen when the nucleus moves by as little as 2 µm (Fig. 1b). For both apparent nucleus sizes, the estimated signal is reduced by 70% if cells are shifted by 5 µm from their initial position.

Three videos (cf. supplementary data, video 1, video 2 and video 3) show the fluorescence signal enhancement due to US-mediated cell uptake and subsequent DNA binding of SYTOX Green intercalating dye. The center of each yellow circle is the intensity-weighted center of mass of the detected cell nucleus; the motion of each cell nucleus is clearly noticeable by following the position of the yellow circle changing during the 9-minute video. The distribution of the maximum nucleus displacements in this time indicates that 89% of the remaining nucleus subpopulation (n=370, after removal of merging cases and pathological cases detected by the operator) had a displacement longer than 2 µm, underlining the need for cell nucleus tracking.

Nucleus detection analysis

Their approximately circular shape allowed detecting the cell nuclei by applying the RST algorithm, without prior knowledge of where the cells are located in the field of view. The RST detected 227, 133 and 168 cell nuclei in the experiment 1, 2 and 3, respectively (Fig 3), thus 528 cells in total. Of these, 21% were cells that merged during the time series (Fig. 3). In

addition, 9% were excluded by the operator because they met one of the rejection criteria mentioned above.

Signal profiles

Representative signal profiles (Fig. 4) show a remarkable difference between processing with and without tracking. First, since the nuclei are detected at the end of the time series and then tracked in the time-reversed sense, the signal collected at the end of the sequence was the same with or without tracking. Then, going backwards in time, nucleus motion induced artificial signal loss when the ROI remained stationary, which can be clearly seen by comparison with the curve where the ROI stayed locked on to the cell (Fig. 4a-b). This ROI tracked the cell nucleus until a detection limit.

The onset of fluorescence signal enhancement was detected noticeably earlier when the nuclei were tracked (Fig. 4a-d). An example of enhancement that well matched the two-compartment model is shown in Fig. 4a, in this case the uptake time constant $1/k = 66.5$s ($r^2 = 0.985$). Tracking also prevented the signal monitoring from signal artifacts caused by the arrival of another nucleus in a stationary ROI (Fig. 4b). For this example, however, the signal enhancement did not obey the two-compartment model, despite this correction, which was probably due to the photobleaching effect leading to signal decay after 5 minutes of acquisition. Furthermore, an example of a nucleus rejected by the operator is shown in Fig. 4c; its signal profile showed abrupt fluctuations, suggesting an oscillating position of the intensity-weighted center of mass, due to the proximity of two cells that could not be resolved by the RST as implemented.

Pharmacokinetic parameters

After automatic removal of the cases of merging cells as well as manual exclusion of the cases listed above during operator verification, the applicability of the two-compartment model was evaluated for the remaining cell population, i.e. 370 nuclei. In this dataset, we analyzed the distribution in saturation signal and uptake rate 1/k, as they were determined with the two-compartment model (Fig. 5). 93% showed a signal variation that was well described by a two-compartment model ($r^2 > 0.95$) (Fig. 3). For all individual experiments, the median value of the uptake time constant 1/k was lower, as well as more homogeneous with tracking, 2'14" (1'29", n=370), than without tracking, 3'17" (3'28", n=370) (Fig. 5, bottom row). Regarding the saturation signal, the bias of the median when tracking is not applied is 6% (30, n=370) (Fig. 5, top row).

With tracking, the detection of the uptake onset occurred earlier with more homogeneous distributions, 2" (2", n=370), than without tracking, 3" (4", n=370) (Fig. 6), further confirming the tight relation with US onset. The difference between these situations is that a ROI was used from the first detection by the RST algorithm or from the end of the time series, respectively. The time of fluorescence onset was detected using a stationary ROI below the detection limit, as described in the methods section. 75% of the nuclei already expressed an uptake onset 4" after US onset and 90% 7s after US onset (Fig. 6).

Potential for an automated SNT

The verification step by the operator showed that manually rejecting nuclei of interest did not lead to any significant difference in any of the data sets; Neither in the saturation signal ($p = 0.53$), nor in the uptake rate ($p = 0.638$) (cf. supplementary data, Fig. 1). Thus, the verification

step conducted by the operator could be skipped since it does not have a significant impact on the resulting pharmacokinetic parameters.

Discussion

Assessment of pharmacokinetic parameters of drugs and hydrophilic model drugs upon plasma membrane sonoporation is of special interest in the domain of US-mediated drug delivery. In a previous study [17], we demonstrated the feasibility of monitoring in real-time the US-mediated intracellular delivery of a model drug using FCFM. Here, we present a complete methodology, including cell nucleus detection and nucleus tracking, which specifically improves the assessment of uptake pharmacokinetic parameters, by removing the biases introduced by cell nucleus motion.

The cell nuclei in these FCFM datasets present as circular bodies with changing diameter and intensity, with slow motion and potentially high density, e.g. 200 nuclei here. In contrast to the majority of articles reporting on single particle tracking [18][23][24], whose purpose is to assess motion aspects of a population of single particles, i.e. motility, diffusivity and velocity [24], the key information we aim to collect by using the tracking algorithm is the fluorescence signal of each cell nucleus of the image. This then allows calculating the uptake kinetics of SYTOX Green fluorescent dye, the model drug used in this sonoporation study. To ensure a convenient workflow and potentially automate the data analysis entirely, the whole processing chain was implemented in single programming environment, from the pre-processing of a high number of images to the assessment of two-compartment based pharmacokinetic parameters for each nucleus. To our knowledge, the single-particle tracking tools available online [24] do not fulfill the requirements of our specific application.

Temporal averaging and anisotropic (SUSAN) filtering preceded nucleus detection, in order to improve the sensitivity, especially for the early signal enhancement directly after the onset of dye uptake, by improving the SNR of the fluorescence images. Cell nuclei were detected by means of the RST-based algorithm [20][21]. Quality of nucleus detection is critical and determines the tracking robustness, i.e. an accurate fluorescence signal monitoring. Since our

investigation focuses on the monitoring of a fluorescence signal enhancement, RST-based nucleus detection overcomes the two following shortcomings: 1) by means of spatial intensity-based gradient images, we can use a single set of RST parameters for this sequence even as signal evolved, 2) neighbor counting of the RST is well adapted to the detection of circular entities, and thus suitable for cell nucleus detection in our application. These two properties of the RST enabled detection of nuclei at an early stage of model drug uptake with a single set of detection parameters.

From the matrix computed by the RST, we set an arbitrary threshold on each frame in order to compute a mask and identify each nucleus. This threshold was set to balance the early detection of nuclei while minimizing the number of merging cases. The spatial resolution of the FCFM microscope, i.e. 3.9 µm, and its 600x500 µm field of view allowed us to monitor a cell population comprising over a hundred nuclei after automatic removal of the merging cases and verification by the operator.

Despite the slow motion of the nuclei all over the sequence, we demonstrated the need for nucleus tracking; The motion of a 4 µm-diameter nucleus that is not tracked led to a 20 % signal loss as soon as it moved by 2 µm, which was the case for 88% of the nuclei contributing to the statistical results. The cell nucleus tracking was based on the ICP [22] method, since the acquisition frame rate was high enough for the mobility of the nuclei. Tracking and analysis required the management of appearing cell nuclei and merged nuclei that are identified as one by the RST. Partly related to the spatial resolution of the acquisition, the tracking software was not capable of separately detecting nuclei that were too close to be resolved from the beginning to the end of the sequence. This required a verification step performed by the operator. The cases identified by the operator did not exceed 8% (5.3, n=3) of the total set of nuclei, and these had a non-significant effect on the resulting pharmacokinetic parameters ($p > 0.05$), allowing the automation of the post-processing

without any operator verification. In addition, a way to validate the nucleus tracking was the continuity of the signal profiles for the non-pathological cases.

Nucleus tracking allowed us to collect the fluorescence signal of each nucleus more accurately, by calculating the spatial mean of the signal in 4-pixel radius collection circles, i.e. 41 pixels. This is an improvement over our feasibility study [17], where pharmacokinetic parameters were derived from the maximum signal of each nucleus, without any tracking. The accuracy of this signal definition was rather limited since it decreased as soon as the pixel containing the maximum signal, following the motion of the nucleus, left the stationary ROI.

The final results involved 370 nuclei; Of these, 93% had a signal enhancement that was well described by a two-compartment model. For every pharmacokinetic parameter, each dataset showed more homogeneous values with lower medians when the tracking was performed. Derived from a more accurate signal monitoring, the representative signal profiles (Fig. 3) clearly show more pronounced curvatures with tracking than without, decreasing the uptake time constant 1/k, and thus the median in the cell population: 2’19” with tracking, compared to 3’19” without. Lower median saturation signal was found, also due to the same reason: a +6% bias was introduced when tracking was not performed. Indeed, monitoring of the fluorescence signal at the early stage of the US exposure was improved by applying the SUSAN filter and the RST-based nucleus detection, leading to an earlier detection of the onset of SYTOX Green uptake by cells: 1.8” with tracking, compared to 2.8” without tracking.

This post-processing methodology allows us to accurately assess the pharmacokinetic properties of more than one hundred of cell nuclei densely present in an image sequence. In combination with an imaging system with higher resolution, the detection and the tracking steps of this methodology could potentially also have value for analysis of e.g. molecular motors [25] or endocytic vesicles that also present as circular shapes. The diameter of the

entities to detect can be set in our pipeline, which makes this detection algorithm extensible for other applications.

Here, we did not take the photobleaching effect into account. Evaluating its effect on the resulting pharmacokinetic parameters could be considered by using a three-compartment model, with a third compartment emptying the second compartment with a single exponential decay [26].

Conclusion

In conclusion, we established a complete post-processing methodology, including cell nucleus detection and nucleus tracking, and demonstrated that this improved the accuracy of the uptake pharmacokinetic parameters assessed in a population of more than one hundred of cells. With the application of the tracking, 93% of the 370 nuclei showed a fluorescence signal variation that was well described by a two-compartment model. This study extends the proof of concept of designing an *in vitro* setup for the real-time monitoring of an US-mediated model drug uptake proposed in Derieppe *et al.* [17]. This setup, together with its post-processing methodology, help decipher kinetic aspects of US- and microbubble-mediated plasma membrane permeabilization, whose knowledge is of special interest in drug delivery of hydrophilic and intercalating anticancer agents.

Acknowledgements

These studies were supported by EU project SonoDrugs (FP7-NMP4-LA-2008-213706), and ERC project 268906 "Sound Pharma".

Conflict of interest

The authors declare that they have no conflict of interest.

References

[1] R. K. Jain, “Delivery of molecular and cellular medicine to solid tumors,” *Advanced Drug Delivery Reviews*, vol. 46, no. 1–3, pp. 149–168, Mar. 2001.

[2] D. Outomuro, D. R. Grana, F. Azzato, and J. Milei, “Adriamycin-induced myocardial toxicity: New solutions for an old problem?,” *International Journal of Cardiology*, vol. 117, no. 1, pp. 6–15, Apr. 2007.

[3] A. A. Manzoor, L. H. Lindner, C. D. Landon, J.-Y. Park, A. J. Simnick, M. R. Dreher, S. Das, G. Hanna, W. Park, A. Chilkoti, G. A. Koning, T. L. M. ten Hagen, D. Needham, and M. W. Dewhirst, “Overcoming Limitations in Nanoparticle Drug Delivery: Triggered, Intravascular Release to Improve Drug Penetration into Tumors,” *Cancer Res*, vol. 72, no. 21, pp. 5566–5575, Nov. 2012.

[4] L. Li, T. L. M. Ten Hagen, M. Bolkestein, A. Gasselhuber, J. Yatvin, G. C. van Rhoon, A. M. M. Eggermont, D. Haemmerich, and G. A. Koning, “Improved intratumoral nanoparticle extravasation and penetration by mild hyperthermia,” *J Control Release*, Feb. 2013.

[5] E. Neumann, S. Kakorin, and K. Tœnsing, “Fundamentals of electroporative delivery of drugs and genes,” *Bioelectrochemistry and Bioenergetics*, vol. 48, no. 1, pp. 3–16, février 1999.

[6] J. Teissie, M. Golzio, and M. Rols, “Mechanisms of cell membrane electropermeabilization: a minireview of our present (lack of?) knowledge,” *Biochimica et Biophysica Acta (BBA)-General Subjects*, vol. 1724, no. 3, pp. 270–280, 2005.

[7] D. M. Skauen and G. M. Zentner, “Phonophoresis,” *International Journal of Pharmaceutics*, vol. 20, no. 3, pp. 235–245, Juillet 1984.

[8] M. W. Miller, D. L. Miller, and A. A. Brayman, “A review of in vitro bioeffects of inertial ultrasonic cavitation from a mechanistic perspective,” *Ultrasound in Medicine & Biology*, vol. 22, no. 9, pp. 1131–1154, 1996.

[9] S. Mitragotri, “Healing sound: the use of ultrasound in drug delivery and other therapeutic applications,” *Nature Reviews Drug Discovery*, vol. 4, no. 3, pp. 255–260, 2005.

[10] R. Y. Tsien, “Imagining imaging’s future,” *Nature Cell Biology*, vol. 5, no. 9; SUPP/1, 2003.

[11] K. Jaqaman, D. Loerke, M. Mettlen, H. Kuwata, S. Grinstein, S. L. Schmid, and G. Danuser, “Robust single-particle tracking in live-cell time-lapse sequences,” *Nature Methods*, vol. 5, no. 8, pp. 695–702, Jul. 2008.

[12] T. Stepanova, J. Slemmer, C. C. Hoogenraad, G. Lansbergen, B. Dortland, C. I. D. Zeeuw, F. Grosveld, G. van Cappellen, A. Akhmanova, and N. Galjart, “Visualization of Microtubule Growth in Cultured Neurons via the Use of EB3-GFP (End-Binding Protein 3-Green Fluorescent Protein),” *J. Neurosci.*, vol. 23, no. 7, pp. 2655–2664, Apr. 2003.

[13] D. Vercauteren, H. Deschout, K. Remaut, J. F. . Engbersen, A. T. Jones, J. Demeester, S. C. De Smedt, and K. Braeckmans, “Dynamic Colocalization Microscopy to Characterize Intracellular Trafficking of Nanomedicines,” *ACS nano*, 2011.

[14] M. J. Saxton and K. Jacobson, “Single-particle tracking: Applications to Membrane Dynamics,” *Annual Review of Biophysics and Biomolecular Structure*, vol. 26, no. 1, pp. 373–399, 1997.

[15] J. Essers, A. B. Houtsmuller, L. van Veelen, C. Paulusma, A. L. Nigg, A. Pastink, W. Vermeulen, J. H. J. Hoeijmakers, and R. Kanaar, “Nuclear dynamics of RAD52 group homologous recombination proteins in response to DNA damage,” *The EMBO Journal*, vol. 21, no. 8, pp. 2030–2037, Apr. 2002.

[16] C. Molenaar, K. Wiesmeijer, N. P. Verwoerd, S. Khazen, R. Eils, H. J. Tanke, and R. W. Dirks, “Visualizing telomere dynamics in living mammalian cells using PNA probes,” *The EMBO Journal*, vol. 22, no. 24, pp. 6631–6641, Dec. 2003.

[17] M. Derieppe, A. Yudina, M. Lepetit-Coiffé, B. de Senneville, C. Bos, and C. Moonen, “Real-Time Assessment of Ultrasound-Mediated Drug Delivery Using Fibered Confocal Fluorescence Microscopy,” *Molecular Imaging and Biology*, pp. 1–9.

[18] E. Meijering, I. Smal, and G. Danuser, “Tracking in molecular bioimaging,” *IEEE Signal Processing Magazine*, vol. 23, no. 3, pp. 46– 53, May 2006.

[19] S. M. Smith and J. M. Brady, “SUSAN—A new approach to low level image processing,” *International journal of computer vision*, vol. 23, no. 1, pp. 45–78, 1997.
[20] G. Loy and A. Zelinsky, “Fast radial symmetry for detecting points of interest,” *Pattern Analysis and Machine Intelligence, IEEE Transactions on*, vol. 25, no. 8, pp. 959–973, 2003.
[21] H. J. Kuijf, J. de Bresser, M. I. Geerlings, M. M. A. Conijn, M. A. Viergever, G. J. Biessels, and K. L. Vincken, “Efficient detection of cerebral microbleeds on 7.0 T MR images using the radial symmetry transform,” *NeuroImage*, vol. 59, no. 3, pp. 2266–2273, février 2012.
[22] N. Cressie, *Statistics for Spatial Data*, Revised Edition. Wiley-Interscience, 1993.
[23] J. Suh, M. Dawson, and J. Hanes, “Real-time multiple-particle tracking: applications to drug and gene delivery,” *Advanced Drug Delivery Reviews*, vol. 57, no. 1, pp. 63–78, Jan. 2005.
[24] E. Meijering, O. Dzyubachyk, and I. Smal, “Methods for cell and particle tracking,” *Methods Enzymol*, vol. 504, no. 9, pp. 183–200, 2012.
[25] V. Levi and E. Gratton, “Exploring dynamics in living cells by tracking single particles,” *Cell Biochemistry and Biophysics*, vol. 48, no. 1, pp. 1–15, 2007.
[26] I. Smal, W. Niessen, and E. Meijering, “Advanced particle filtering for multiple object tracking in dynamic fluorescence microscopy images,” in *Biomedical Imaging: From Nano to Macro, 2007. ISBI 2007. 4th IEEE International Symposium on*, 2007, pp. 1048–1051.

Figures

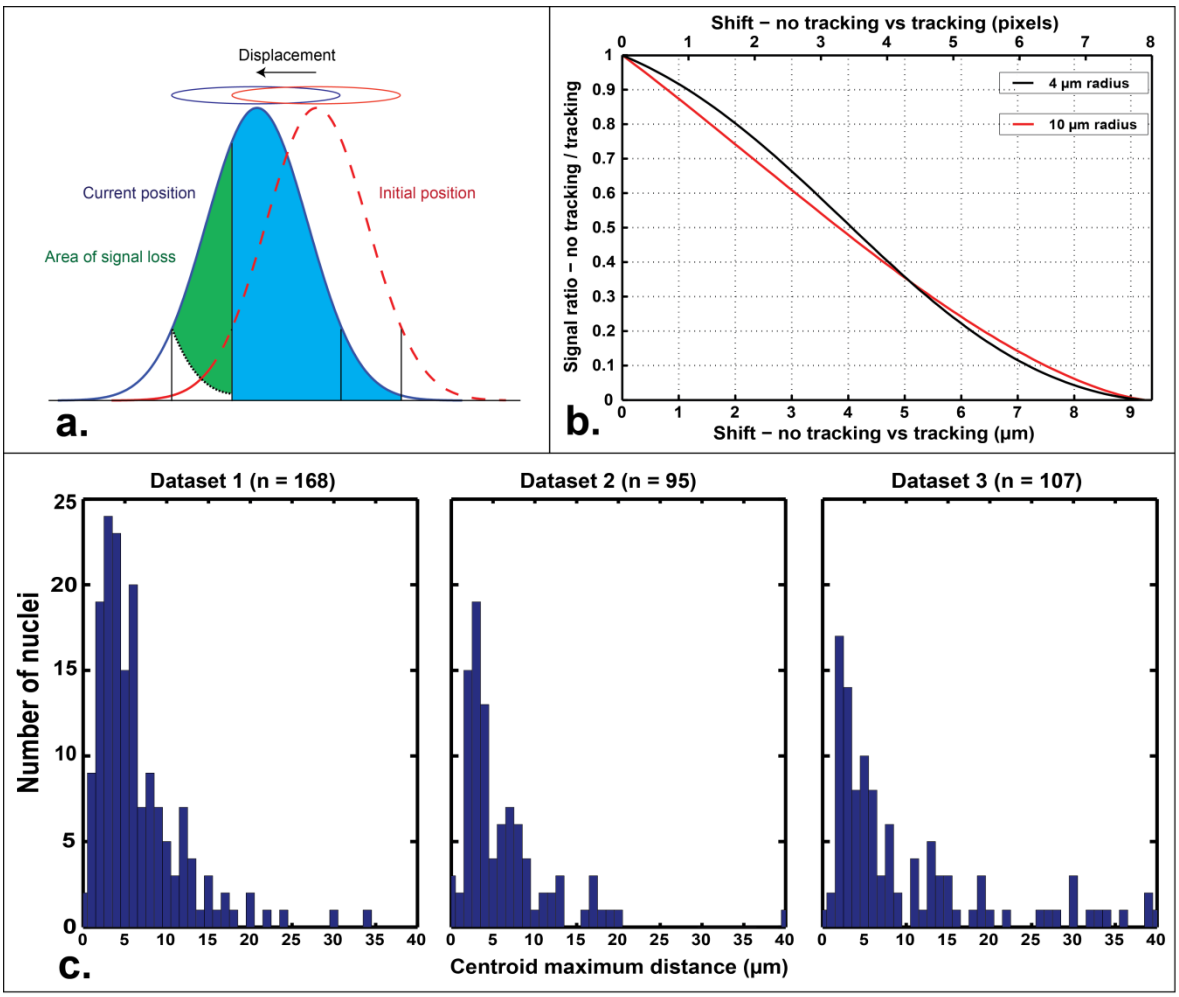

Figure 1. *Impact of nucleus displacement on the measured signal.* ***a*** *Schematic of a cell nucleus at its current (blue profile) and initial position (red dashed profile). The nucleus fluorescence signal is assumed to be Gaussian with a 7 µm full width at half maximum. A circular ROI of 4.8 µm radius (blue circle) is centered on the current position. Without tracking, however, signal is collected from the ROI at its initial position (red circle). In this case, only the blue area is accounted for and a noticeable signal loss (green area) is incurred, compared to the situation in which the nucleus is tracked.* ***b*** *Signal ratio – signal without tracking/signal with tracking – as a function of the distance separating the centers of the collection circles in each configuration.* ***c*** *Histograms of the maximum distance of the intensity-weighted centers of mass, for each dataset.*

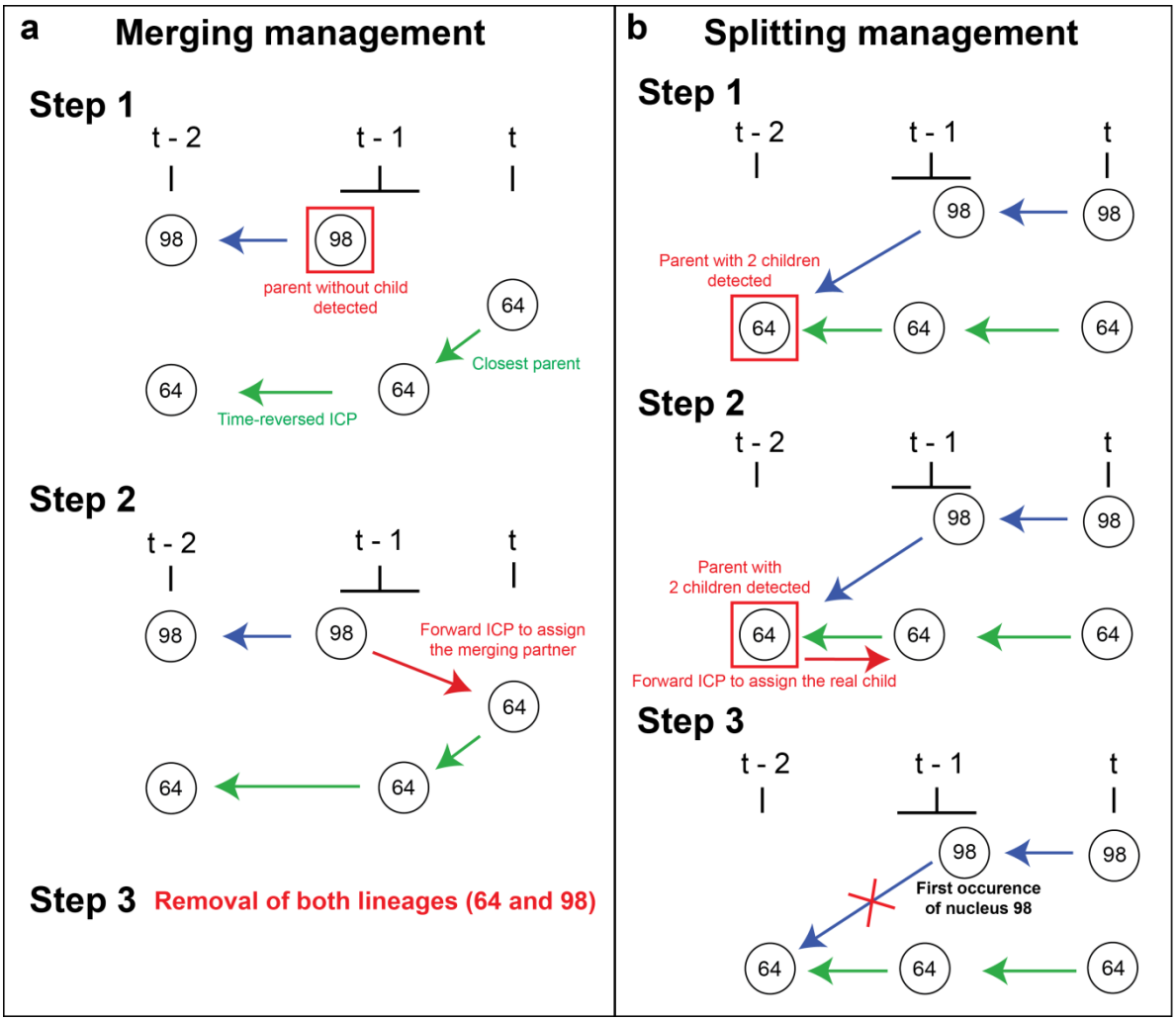

Figure 2. *Management of merging and splitting.* ***a*** *Detection and removal of the cases of merging.* ***b*** *Detection and management of the cases of splitting.*

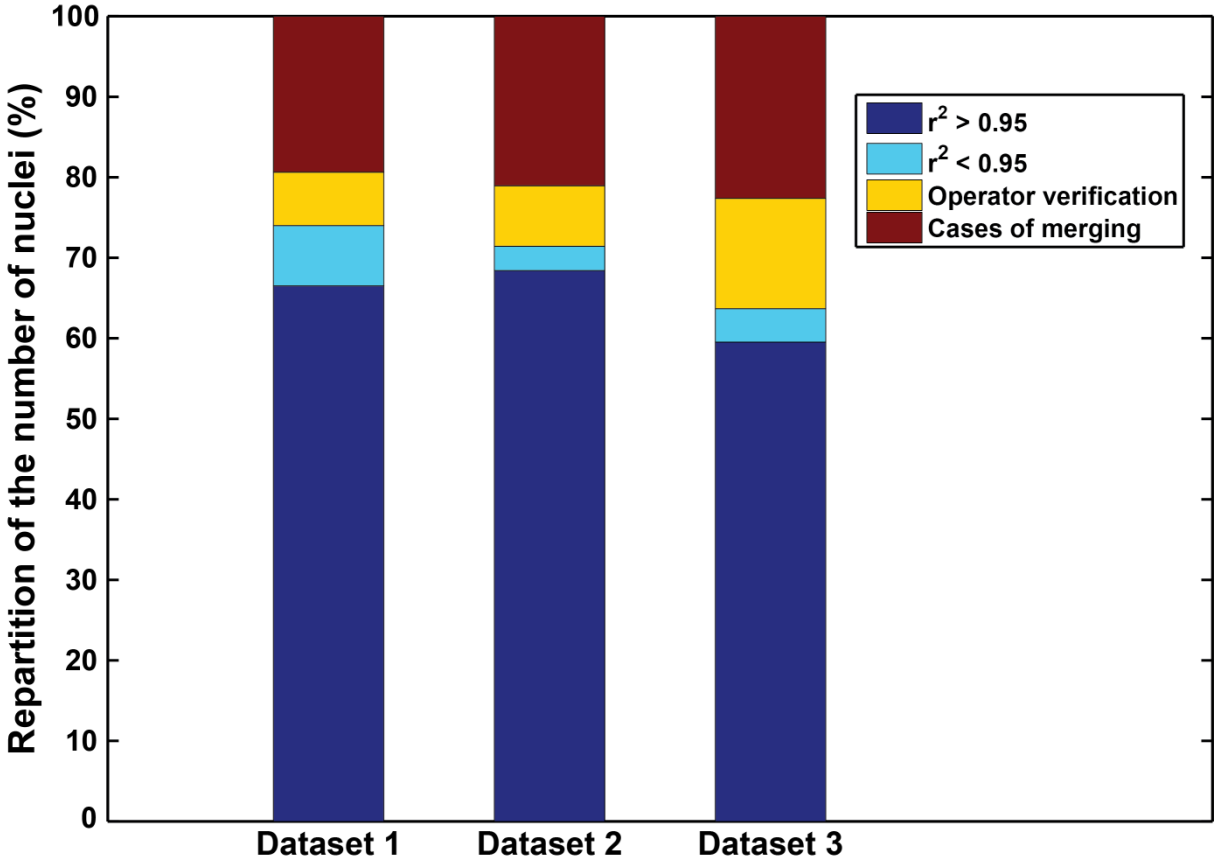

Figure 3. *Proportion of the number of nuclei that were managed in each step of the workflow, for each dataset.*

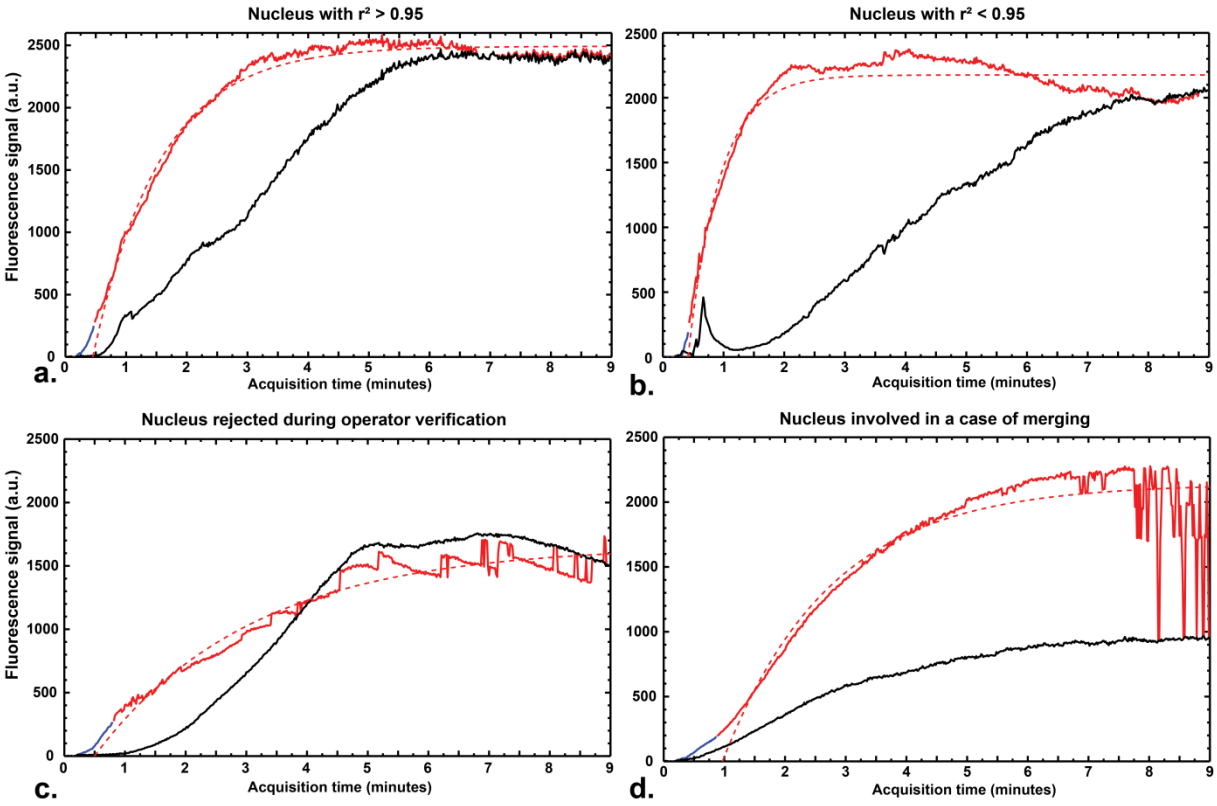

Figure 4. *Mean fluorescence signal intensity as a function of the acquisition time of representative nuclei, one case randomly chosen from each category in figure 3. ,The signal profiles obtained with tracking (solid red lines – dashed red line for the corresponding fit) benefit from a signal gain with a higher sensitivity to the curvature of the exponential and an earlier detection of the signal onset, compared to those obtained without tracking (solid black lines).* ***a*** *Case of an included nucleus with* r^2*>0.95 (Fig. 3 – dark blue subpopulation). With tracking 1/k = 1'06" (*r^2 *= 0.985).* ***b*** *Case of a included nucleus with* r^2*<0.95 (Fig .3 – light blue subpopulation). With tracking 1/k = 0'31" (*r^2 *= 0.896).* ***c*** *Case of a nucleus rejected by the operator: these were 2 cells merged from the beginning to the end (Fig. 2 – yellow subpopulation). With tracking 1/k = 2'36" (*r^2 *= 0.947).* ***d*** *Case of an excluded nucleus that was automatically rejected because of merging (Fig. 2 – red subpopulation). With tracking 1/k= 1'46" (*r^2 *= 0.887).*

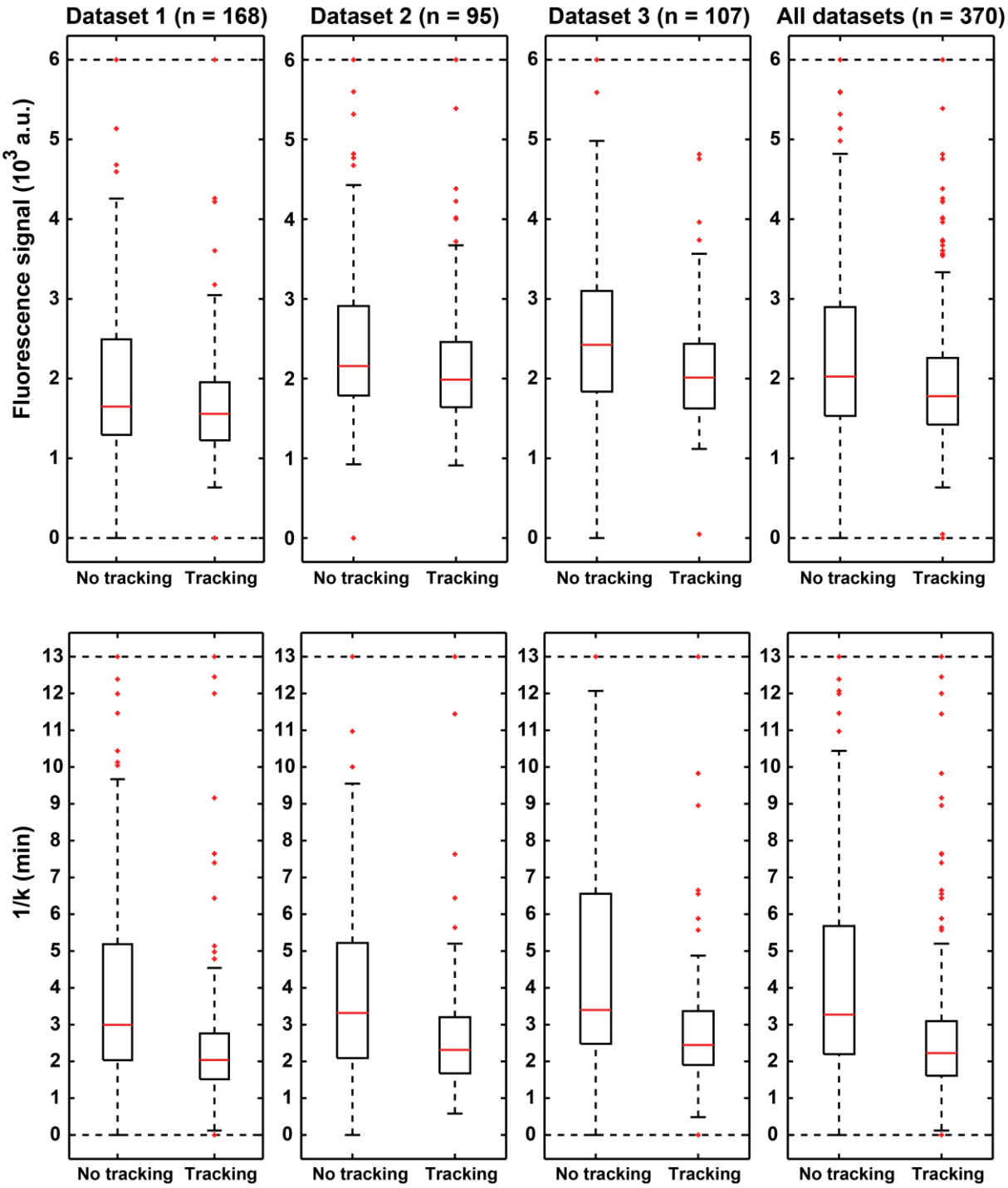

Figure 5. *Boxplots of the kinetic parameters obtained with the two-compartment model: Signal enhancement asymptote (top row) and uptake time constant 1/k (bottom row) for each dataset (column 1, 2 and 3), and the accumulation of all the datasets (column 4). In each case, the results without tracking (left) are compared to those with tracking (right).*

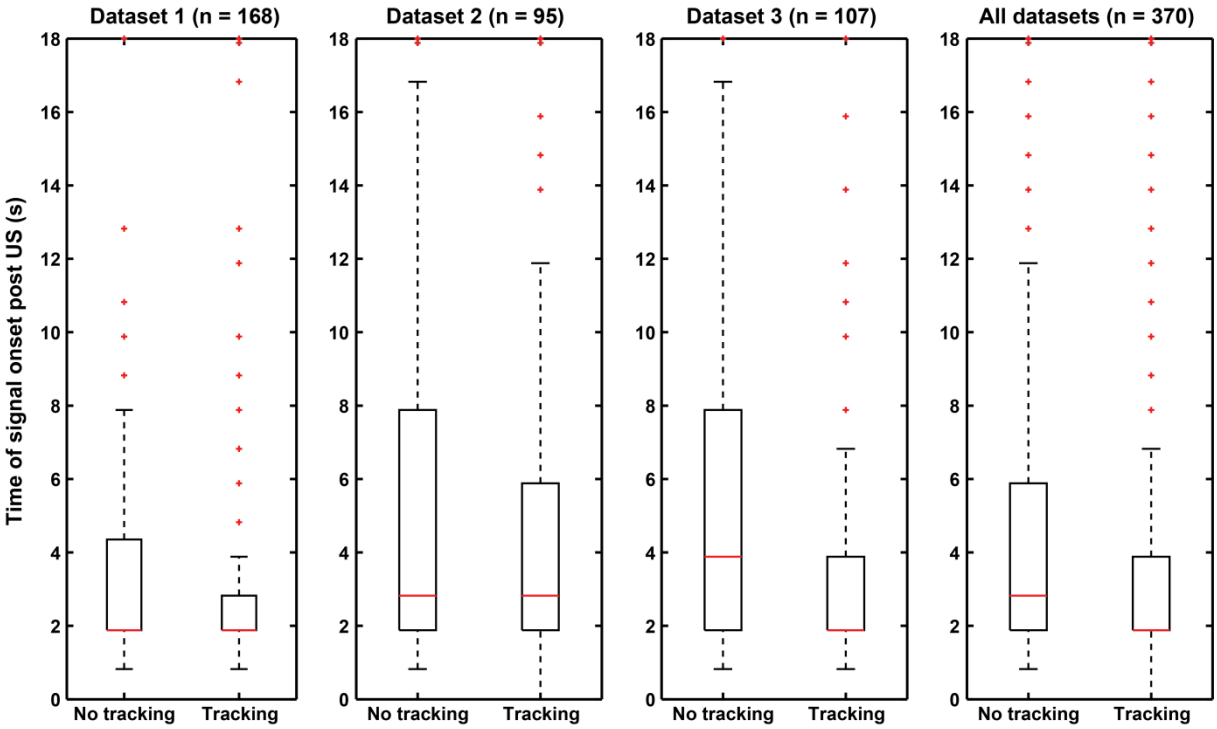

Figure 6. *Boxplots of the time of the uptake onset.*

Supplementary data

Table 1 – Supplementary data. *Values of pharmacokinetic parameters for each dataset.*

Pharmacokinetic parameter		**Asymptotic signal enhancement (*A*)**		**Time of fluorescence signal onset (*T*)**		**Uptake rate constant (1/*k*)**	
Condition		**Without tracking**	**With tracking**	**Without tracking**	**With tracking**	**Without tracking**	**With tracking**
Dataset 1 (n = 168)	**Median**	1649	1558	1”9	1”9	3’00”	2’02”
	IR (abs/%)	1198/**73**	728/**63**	2”5/**132**	0”9/**47**	3’09”/**105**	1’15”/**61**
Dataset 2 (n = 95)	**Median**	2157	1987	2”8	2”8	3’19”	2’19”
	IR (abs/%)	1122/**52**	819/**41**	5”7/**204**	4”0/**143**	3’08”/**94**	1’32”/**66**
Dataset 3 (n = 107)	**Median**	2424	2013	3”9	1”9	3’24”	2’27”
	IR (abs/%)	1263/**52**	811/**40**	6”0/**154**	2”0/**105**	4’05”/**120**	1’28”/**60**
All datasets (n = 370)	**Median**	2025	1779	2”8	1”9	3’16”	2’14”
	IR (abs/%)	1366/**67**	836/**47**	4”0/**143**	2”0/**105**	3’29”/**107**	1’29”/**66**
	p-value	Different: < 0.0001		Different: < 0.0001		Different: < 0.0001	

Table 2 - Supplementary data. *Comparison of the distributions of uptake rate 1/k before and after removal of the cases rejected by the operator.*

Uptake rate 1/*k* with tracking		**Uptake rate constant (1/*k*)**	
		Before removal	**After removal**
Dataset 1	**n**	183	168
	Median	2”01	2”02
	IR (abs/%)	1”22/**68**	1”15/**61**
Dataset 2	**n**	105	95
	Median	2”20	2”19
	IR (abs/%)	1”36/**69**	1”32/**66**
Dataset 3	**n**	130	107
	Median	2”24	2’27”
	IR (abs/%)	1”41/**70**	1’28”/**60**
All datasets	**n**	418	370
	Median	2’13”	2’14”
	IR (abs/%)	1”34/**71**	1’29”/**66**
	p-value	**Non significant p = 0.638**	

Note: the percentage of interquartile range is calculated as follows: $IR\ (\%) = \frac{IR\ (absolute)}{median}$

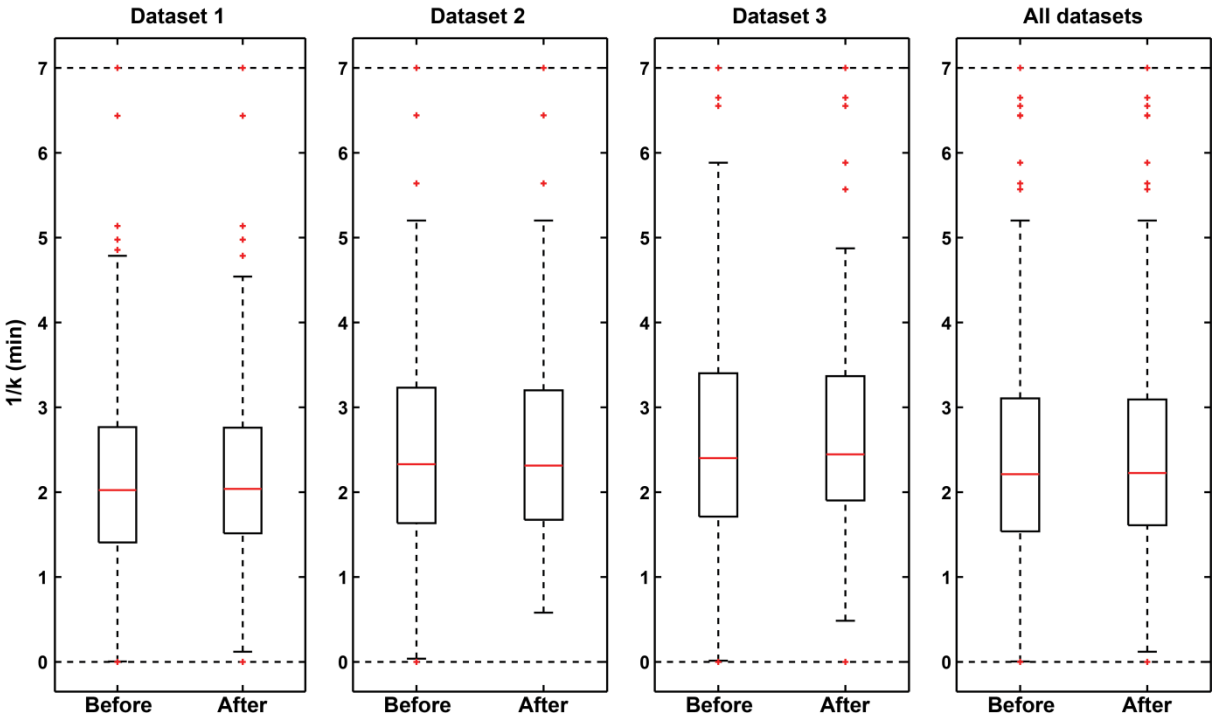

Figure 1 - Supplementary data. *Comparison of the distributions of uptake rate 1/k before and after removal of the cases rejected by the operator.*